JOC Article

New Chromogenic and Fluorescent Probes for Anion Detection: Formation of a [2 + 2] Supramolecular Complex on Addition of Fluoride with Positive Homotropic Cooperativity

Chan-Yu Chen,[†,‡] Tzu-Pin Lin,[†] Chine-Kun Chen,[†,‡] Su-Ching Lin,[†] Mei-Chun Tseng,[†] Yuh-Sheng Wen,[†] and Shih-Sheng Sun*[,†]

Institute of Chemistry, Academia Sinica, 115 Nankang, Taipei, Taiwan, Republic of China, and Department of Chemistry, National Central University, 320 Chungli, Taiwan, Republic of China

sssun@chem.sinica.edu.tw

Received September 17, 2007

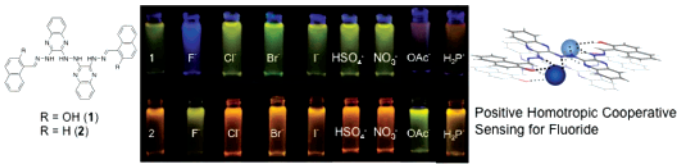

Two new chromogenic and fluorescent probes for anions have been designed, synthesized, and characterized. These probes contain multiple hydrogen bonding donors including hydrazine, hydrazone, and hydroxyl functional groups for potential anion interacting sites. Despite the possible flexible structural framework due to the presence of sp^3 carbon linkage, X-ray structure analysis of probe **2** displayed an essentially planar conformation in the solid state owing to strong crystal packing interactions comprising a combination of favorable $\pi-\pi$ stacking effect and hydrogen bonding to cocrystallized CH_3OH molecules. Both probes **1** and **2** display orange color in DMSO solution and show fairly weak fluorescence at room temperature. Binding studies revealed that both probes **1** and **2** show noticeable colorimetric and fluorescent responses only to F^-, OAc^-, and $H_2PO_4^-$ among the nine anions tested (F^-, Cl^-, Br^-, I^-, OAc^-, $H_2PO_4^-$, HSO_4^-, ClO_4^-, and NO_3^-). The general trend of the sensitivity to anions follows the order of $F^- > OAc^- > H_2PO_4^- > Cl^- > Br^- \approx I^- \approx HSO_4^- \approx ClO_4^- \approx NO_3^-$. A 1:2 (probe to anion) binding stoichiometry was found for probe **1** with OAc^- and $H_2PO_4^-$ and probe **2** with F^-, OAc^-, and $H_2PO_4^-$. The binding isotherm of probe **1** to F^- was found to be complicated with apparent multiple equilibria occurring in solution. The formation of an aggregated supramolecular complex upon addition of fluoride is proposed to rationalize the observed optical responses and is supported by ESI mass spectrometry and pulsed-field gradient NMR spectroscopy. Data analysis suggests that the binding of probe **1** to F^- shows positive homotropic cooperativity.

Introduction

The development of chromogenic and fluorogenic chemosensors for molecular sensing is an area of current interest.[1] Among the various recognition modes of receptor−analyte interactions, the utilization of cooperative interaction or allosteric regulation of binding affinity of a receptor toward specific analytes that mimics the binding processes in nature represents an attractive direction in designing novel chemosensors and has recently received increasing attention.[2] Cooperativity is a common phenomenon occurring in biological enzyme−substrate interactions and catalysis. Several artificial cooperative receptors have been designed accordingly for a variety of analytes,[2−4] though very few successful examples have been further developed for anion sensing purposes.[4]

The capability of specific detection of inorganic anions is critical in terms of their important roles in biological, environmental, and industrial processes. Notable examples of neutral anion receptors in the literature comprise amide, sulfonamide,

[†] Academia Sinica.
[‡] National Central University.

(1) (a) Martínez-Máñez, R.; Sancenón, F. *Chem. Rev.* **2003**, *103*, 4419−4476 and references cited therein. (b) Amendola, V.; Esteban-Gómez, D.; Fabbrizzi, L.; Licchelli, M. *Acc. Chem. Res.* **2006**, *39*, 343−353 and references cited therein.

(2) (a) Takeuchi, M.; Ikeda, M.; Sugasaki, A.; Shinkai, S. *Acc. Chem. Res.* **2001**, *34*, 865−873. (b) Kovbasyuk, L.; Krämer, R. *Chem. Rev.* **2004**, *104*, 3161−3187 and references cited therein. (c) Perutz, M. F. *Annu. Rev. Biochem.* **1979**, *48*, 327−386.

10.1021/jo7019916 CCC: $40.75
Published on Web 01/10/2008

SCHEME 1

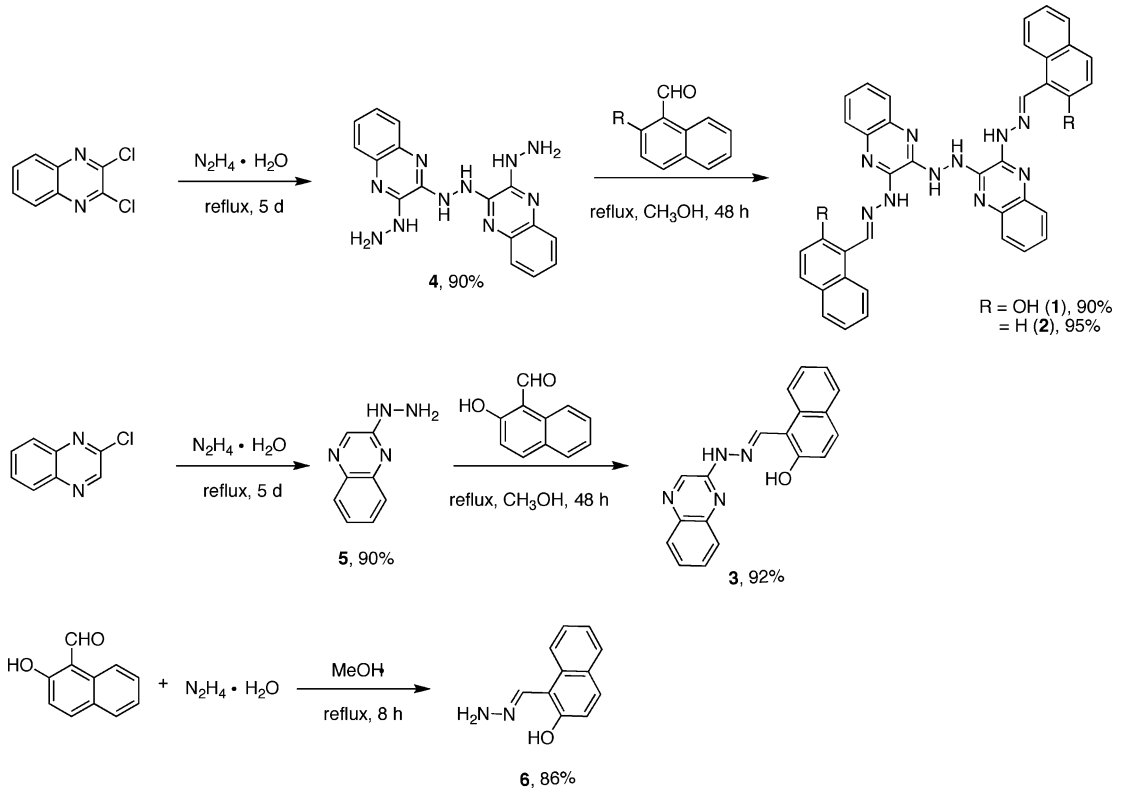

pyrrole, urea, thiourea, and guanidinium groups as binding sites which are able to establish N−H···A$^-$ hydrogen bonds with anions.[1,5] The aryl C−H···anion hydrogen bonding may also participate in the collective interactions with appropriate design of the host molecules.[6] In some extreme cases, the basic anion-induced deprotonation from polarized acidic protons occurs.[1b,7]

On the other hand, the examples of utilization of polarized hydrazone and hydrazine N−H to direct the hydrogen bonding with anions are surprisingly few,[8] partly due to the high pK_a values found in typical hydrazone and hydrazine N−Hs and, therefore, the inability to establish strong hydrogen bonding

(3) (a) Pérez, E. M.; Sánchez, L.; Fernández, G.; Martín, N. *J. Am. Chem. Soc*. **2006**, *128*, 7172−7173. (b) Sessler, J. L.; Tomat, E.; Lynch, V. M. *J. Am. Chem. Soc*. **2006**, *128*, 4184−4185. (c) Le Gac, S.; Marrot, J.; Reinaud, O.; Jabin, I. *Angew. Chem., Int. Ed.* **2006**, *45*, 3123−3126. (d) Heo, J.; Mirkin, C. A. *Angew. Chem., Int. Ed.* **2006**, *45*, 941−944. (e) Yan, Z.; Chang, Y.; Mayo, D.; Maslak, V.; Xia, S.; Badjic, J. D. *Org. Lett.* **2006**, *8*, 3697−3700. (f) Wang, J.; Qian, X. *Org. Lett.* **2006**, *8*, 3721−3724. (g) Varghese, R.; George, S. J.; Ajayaghosh, A. *Chem. Commun.* **2005**, 593−595. (h) Sato, H.; Tashiro, K.; Shinmori, H.; Osuka, A.; Murata, Y.; Komatsu, K.; Aida, T. *J. Am. Chem. Soc*. **2005**, *127*, 13086−13087. (i) Gianneschi, N. C.; Nguyen, S. T.; Mirkin, C. A. *J. Am. Chem. Soc*. **2005**, *127*, 1644−1645. (j) Thordarson, P.; Coumans, R. G. E.; Elemans, J. A. A. W.; Thomassen, P. J.; Visser, J.; Rowan, A. E.; Nolte, R. J. M. *Angew. Chem., Int. Ed*. **2004**, *43*, 4755−4759. (k) Chang, S.-Y.; Jang, H.-Y.; Jeong, K.-S. *Chem.—Eur. J*. **2004**, *10*, 4358−4366. (l) Thordarson, P.; Bijsterveld, E. J. A.; Elemans, J. A. A. W.; Kasak, P.; Nolte, R. J. M.; Rowan, A. E. *J. Am. Chem. Soc*. **2003**, *125*, 1186−1187. (m) Chen, C.-T.; Huang, W.-P. *J. Am. Chem. Soc*. **2002**, *124*, 6246−6247. (n) Ishi-I, T.; Crego-Calama, M.; Timmerman, P.; Reinhoudt, D. N.; Shinkai, S. *Angew. Chem., Int. Ed*. **2002**, *41*, 1924−1929. (o) Sugasaki, A.; Sugiyasu, K.; Ikeda, M.; Takeuchi, M.; Shinkai, S. *J. Am. Chem. Soc*. **2001**, *123*, 10239−10244.

(4) (a) Tomat, E.; Cuesta, L.; Lynch, V. M.; Sessler, J. L. *Inorg. Chem.* **2007**, *46*, 6224−6226. (b) Lankshear, M. D.; Cowley, A. R.; Beer, P. D. *Chem. Commun.* **2006**, 612−614. (c) Yamaguchi, S.; Yoshimura, I.; Kohira, T.; Tamaru, S.-i.; Hamachi, I. *J. Am. Chem. Soc.* **2005**, *127*, 11835−11841. (d) Hirata, O.; Takeuchi, M.; Shinkai, S. *Chem. Commun*. **2005**, 3805−3807. (e) Boiocchi, M.; Boca, L.; Esteban-Gómez, D.; Fabbrizzi, L.; Licchelli, M.; Monzan, E. *J. Am. Chem. Soc*. **2004**, *126*, 16507−16514. (f) Abouderbala, L. O.; Belcher, W. J.; Boutelle, M. G.; Cragg, P. J.; Steed, J. W.; Turner, D. R.; Wallace, K. J. *Proc. Natl. Acad. Sci. U.S.A.* **2002**, *99*, 5001−5006. (g) Sessler, J. L.; Maeda, H.; Mizuno, T.; Lynch, V. M.; Furuta, H. *J. Am. Chem. Soc*. **2002**, *124*, 13474−13479. (h) Raker, J.; Glass, T. E. *J. Org. Chem*. **2002**, *67*, 6113−6116. (i) Takeuchi, M.; Shioya, T.; Swager, T. M. *Angew. Chem., Int. Ed*. **2001**, *40*, 3372−3376.

(5) (a) Beer, P. D.; Gale, P. A. *Angew. Chem., Int. Ed*. **2001**, *40*, 486−516 and references cited therein. (b) Wu, Y.; Peng, X.; Fan, J.; Gao, S.; Tian, M.; Zhao, J.; Sun, S. *J. Org. Chem.* **2007**, *72*, 62−70. (c) Chen, C.-L.; Lin, T.-P.; Chen, Y.-S.; Sun, S.-S. *Eur. J. Org. Chem*. **2007**, 3999−4010. (d) Chen, C.-L.; Chen, Y.-S.; Chen, C.-Y.; Sun, S.-S. *Org. Lett.* **2006**, *8*, 5053−5056. (e) Nishiyabu, R.; Anzenbacher, P. Jr. *Org. Lett.* **2006**, *8*, 359−362. (f) Turner, D. R.; Paterson, M. J.; Steed, J. W. *J. Org. Chem.* **2006**, *71*, 1598−1608. (g) Miyaji, H.; Kim, H.-K.; Sim, E.-K.; Lee, C.-K.; Cho, W.-S.; Sessler, J. L.; Lee, C.-H. *J. Am. Chem. Soc.* **2005**, *127*, 12510−12512. (h) Anzenbacher, P., Jr.; Palacios, M. A.; Jursíková, K.; Marauez, M. *Org. Lett.* **2005**, *7*, 5027−5030. (i) Kim, S. K.; Bok, J. H.; Bartsch, R. A.; Lee, J. Y.; Kim, J. S. *Org. Lett.* **2005**, *7*, 4839−4842. (j) Liu, B.; Tian, H. *J. Mater. Chem*. **2005**, *15*, 2681−2686. (k) Bondy, C. R.; Gale, P. A.; Loeb, S. J. *J. Am. Chem. Soc*. **2004**, *126*, 5030−5031. (l) Black, C. B.; Andrioletti, B.; Try, A. C.; Ruiperez, C.; Sessler, J. L. *J. Am. Chem. Soc.* **1999**, *121*, 10438−10439. (m) Palacios, M. A.; Nishyabu, R.; Marquez, M.; Anzenbacher, P., Jr. *J. Am. Chem. Soc*. **2007**, *129*, 7538−7544. (n) Nishyabu, R.; Palacios, M. A.; Dehaen, W.; Anzenbacher, P., Jr. *J. Am. Chem. Soc*. **2006**, *128*, 11496−11504.

(6) (a) Belcher, W. J.; Fabre, M.; Farhan, T.; Steed, J. W. *Org. Biomol. Chem.* **2006**, *4*, 781−786. (b) Wallace, K. J.; Belcher, W. J.; Turner, D. R.; Syed, K. F.; Steed, J. W. *J. Am. Chem. Soc*. **2003**, *125*, 9699−9715. (c) Ihm, H.; Yun, S.; Kim, H. G.; Kim, J. K.; Kim, K. S. *Org. Lett.* **2002**, *4*, 2897−2900. (d) Yun, S.; Ihm, H.; Kim, H. G.; Lee, C. W.; Indrajit, B.; Oh, K. S.; Gong, Y. J.; Lee, J. W.; Yoon, J.; Lee, H. C.; Kim, K. S. *J. Org. Chem.* **2003**, *68*, 2467−2470.

(7) (a) Gunnlaugsson, T.; Glynn, M.; Tocci, G. M.; Kruger, P. E.; Pfeffer, F. M. *Coord. Chem. Rev.* **2006**, *250*, 3094−3117. (b) Gunnlaugsson, T.; Kruger, P. E.; Jensen, P.; Tierney, J.; Ali, H. D. P.; Hussey, G. M. *J. Org. Chem*. **2005**, *70*, 10875−10878. (c) Lin, C.-I.; Selvi, S.; Fang, J.-M.; Chou, P.-T.; Lai, C.-H.; Cheng, Y.-M. *J. Org. Chem.* **2007**, *72*, 3537−3542. (d) Lin, T.-P.; Chen, C.-Y.; Wen, Y.-S.; Sun, S.-S. *Inorg. Chem.* **2007**, *46*, 9201−9212. (e) Wu, C.-Y.; Chen, M.-S.; Lin, C.-A.; Lin, S.-C.; Sun, S.-S. *Chem.—Eur. J*. **2006**, *12*, 2263−2269. (f) Esteban-Gómez, D.; Fabbrizzi, L.; Licchelli, M. *J. Org. Chem.* **2005**, *70*, 5717−5720.

TABLE 1. Crystallographic Data for Compounds 2 and 4

	4·2 DMSO	**2**·4CH_3OH
empirical formula	$C_{20}H_{28}N_{10}O_2S_2$	$C_{42}H_{44}N_{10}O_4$
M (g mol^{-1})	504.63	752.87
cryst syst	monoclinic	triclinic
space group	$P2(1)/c$	$P\bar{1}$
a (Å)	11.4642(2)	9.8797(5)
b (Å)	14.3870(3)	12.9092(7)
c (Å)	11.1691(2)	15.6505(8)
α (deg)	90	78.569(3)
β (deg)	117.7010(10)	79.168(4)
γ (deg)	90	76.872(3)
V (Å^3)	1631.04(5)	1883.85(17)
Z	4	2
$R1$ (all, $>2\sigma$)	0.0624, 0.0459	0.1863, 0.0453
$wR2$ (all, $>2\sigma$)	0.1419, 0.1364	0.0672, 0.0539

interaction with anions.[9] Nevertheless, we envision the polarization of the N−H and the anion binding capability could be strengthened with the combination of multiple hydrogen bonding with strong electron-withdrawing substituents and additional $\pi-\pi$ interaction. Herein we report a new type of highly sensitive optical probe for inorganic anions, in particular, for fluoride, featuring strong positive homotropic cooperative interaction through the combination of hydrazine/hydrazone/imine/hydroxyl anion hydrogen bonding and an aromatic $\pi-\pi$ stacking effect.

Results and Discussion

Synthesis and Crystal Structure Analysis. Scheme 1 outlines the synthetic procedures for probes **1** and **2**. The key starting material, 1,2-bis(3-hydrazinylquinoxalin-2-yl)hydrazine (**4**), was prepared in high yield by refluxing 1,2-dichloroquinoxaline in hydrazine. Subsequent condensation of **4** with 2-hydroxy-1-naphthaldehyde or 1-naphthaldehyde in methanol afforded **1** and **2**, respectively, in excellent yields. Compound **3**, which consists of half structural framework of probe **1**, was also synthesized to serve as a comparative model for probe **1**. The phenol proton signals in **1** and **3** display significant downfield shift to 13.1 and 11.9 ppm, respectively, indicating the presence of intramolecular hydrogen bonding between the phenol proton and the imine nitrogen atom. All new compounds have been characterized by NMR spectroscopy, high-resolution mass spectrometry, and elemental analysis. The structures of compounds **2** and **4** are further confirmed by X-ray crystallography. The crystallographic data are summarized in Table 1.

Single crystals of **4** suitable for crystallography were obtained from slow evaporation of a concentrated dimethyl sulfoxide (DMSO) solution of **4** at ambient temperature. The ORTEP structure of **4** is depicted in Figure 1. A C_2 symmetry is presented in the structure. Two DMSO molecules are cocrystallized with **4** in the unit cell. The DMSO molecules are located in the positions where two hydrogen bonds are present between the oxygen atom in DMSO and two hydrazine protons with distances of 2.96 Å (N12H···O) and 3.22 Å (N11H···O).

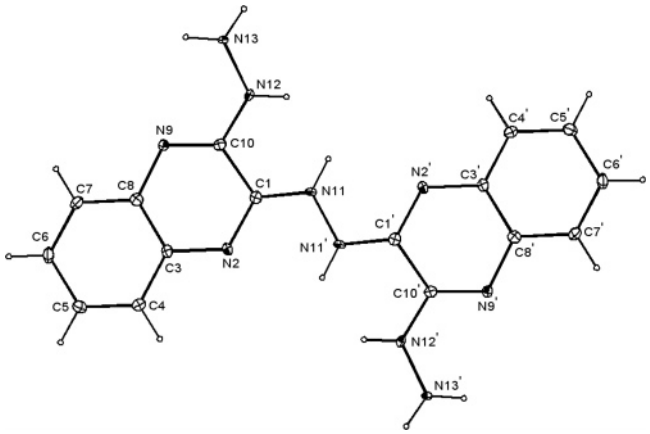

FIGURE 1. The ORTEP drawing of **4**. The thermal ellipsoids are drawn at the 30% probability level.

Figure 2 shows the crystal structure of **2** obtained from slow evaporation of a tetrahydrofuran (THF)/MeOH solution of **2**. It is anticipated that the existence of several single bonds between the aromatic moieties in **2** would result in free rotations of these single bonds in solution. However, it should be noted here that all four aromatic moieties in **2** are aligned in an essentially coplanar fashion with maximum dihedral angle of 7° that indicates a strong crystal packing interaction existing in the solid state. Indeed, the quinoxaline unit and the next adjacent naphthyl unit exhibit notable aromatic $\pi-\pi$ stacking with a distance of 3.42 Å. Moreover, each of the two molecules of **2** forms a pair of substructure with two methanol molecules sandwiched between by formation of a series of hydrogen bonds with the hydrazine and hydrazone N−H groups. The tendency of probe **1** to form aggregated structure is also manifested where not only the monomer itself but also the dimeric (1313.5209, calculated: 1313.4872), trimeric (1970.7771, calculated: 1970.7302), and tetrameric (2627.0176, calculated: 2626.9699) structures can be identified from the obtained high-resolution electrospray ionization (ESI) mass spectrum. The coplanar structure and effective $\pi-\pi$ stacking have found to be a critical feature to their great sensitivity to recognize fluoride.

Photophysical Properties. Table 2 collects the photophysical parameters for **1**−**6** in DMSO solution. Figure 3 illustrates the absorption spectra of compounds **1**−**3**. Both **1** and **2** exhibit a prominent absorption band at ca. 390 nm and a series of vibrational features at ca. 459, 457, and 490 nm. By comparison to the absorption spectra of the model compounds **3** and **6** as well as precursors **4** and **5**, the absorption band of **1** and **2** at ca. 390 nm is tentatively assigned to the $\pi-\pi^*$ transitions localized on the naphthyl imine moiety while the absorption bands at longer wavelength over 400 nm featuring vibrational structures are assigned to the $\pi-\pi^*$ transitions localized on the quinoxaline hydrazine unit.

Both **1** and **2** exhibit fairly weak fluorescence at 542 nm ($\Phi_f = 0.0035$) and 544 nm ($\Phi_f = 0.0020$) in DMSO solution with typical singlet excited-state lifetimes of 140 and 120 ps, respectively. Figure 4 compares the fluorescence spectra of **1** and **2**. Although compound **1** contains the salicylidene hydrazine moiety, which is known for its tendency to proceed via excited-state intramolecular proton transfer (ESIPT) in the $^1\pi\pi^*$ state during the period of low-frequency vibrational motions associ-

(8) (a) Han, F.; Bao, Y.; Yang, Z.; Fyles, T. M.; Zhao, J.; Pemg, X.; Fan, J.; Wu, Y.; Sun, S. *Chem.—Eur. J.* **2007**, *13*, 2880−2892. (b) Zhao, Y.-G.; Zhang, B.-G.; Duan, C.-Y.; Lin, Z.-H.; Meng, Q.-J. *New J. Chem.* **2006**, *30*, 1207−1213. (c) Lin, Z.-H.; Zhao, Y.-G.; Duan, C.-Y.; Zhang, B.-G.; Bai, Z.-P. *Dalton Trans.* **2006**, 3678−3684. (d) Zhao, Y.-G.; Lin, Z.-H.; Ou, S.; Duan, C.-Y.; Liao, H.; Bai, Z.-P. *Inorg. Chem. Commun.* **2006**, *9*, 802−805. (e) Vázquez, M.; Fabbrizzi, L.; Taglietti, A.; Pedrido, R. M.; González-Noya, A. M.; Bermejo, M. R. *Angew. Chem., Int. Ed.* **2004**, *43*, 1962−1965.

(9) (a) Bordwell, F. G. *Acc. Chem. Res.* **1988**, *21*, 456−463. (b) Zhao, Y.; Bordwell, F. G.; Cheng, J.-P.; Wang, D. *J. Am. Chem. Soc.* **1997**, *119*, 9125−9129.

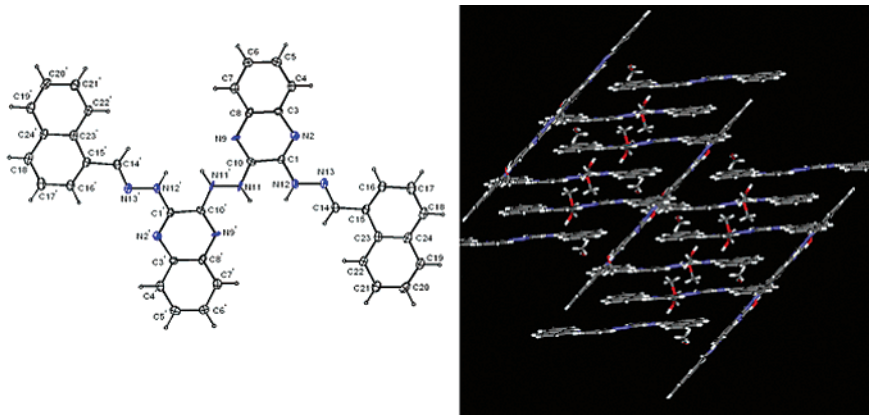

FIGURE 2. Left: the ORTEP drawing of probe **2**. The thermal ellipsoids are drawn at the 30% probability level. Right: the packing diagram of probe **2** showing the $\pi-\pi$ stacking and hydrogen bonding between **2** and methanol.

TABLE 2. Photophysical Properties of Compounds 1−6 in DMSO Solution at 293 K

compound	absorption λ_{max}, nm ($10^{-3}\epsilon$, $M^{-1}cm^{-1}$)	Emission λ_{em}, nm	$10^2\Phi_{em}$	τ, ns
1	325 (22.3), 397 (47.8), 459 (24.6), 490 (15.3)	542	0.35	0.14
2	381 (53.5), 429 (28.0), 457 (28.7), 487 (18.4)	544	0.20	0.12
3	257 (29.1), 322 (13.6), 404 (21.4)	522	0.42	0.11
4	303 (14.1), 364 (10.3), 375 (15.3), 402 (34.8), 426 (42.3), 453 (27.4)	493	0.11	3.4
5	363 (5.21)	394	0.23	4.5
6	309 (10.2), 319 (10.3), 351 (9.60), 363 (9.54)	378, 454	0.0059[a]	1.2[b], 6.3[c]

[a] The total quantum yield. [b] Monitored at 370 nm. [c] Monitored at 470 nm.

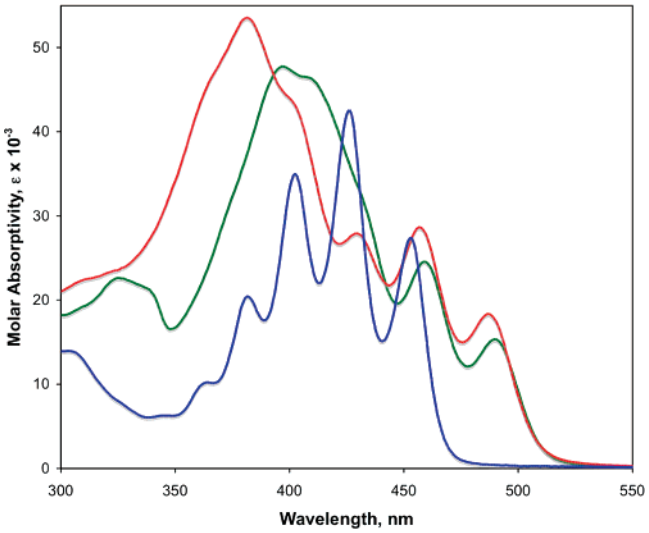

FIGURE 3. The absorption spectra of compounds **1** (green), **2** (red), and **4** (blue) in DMSO solution at 293 K.

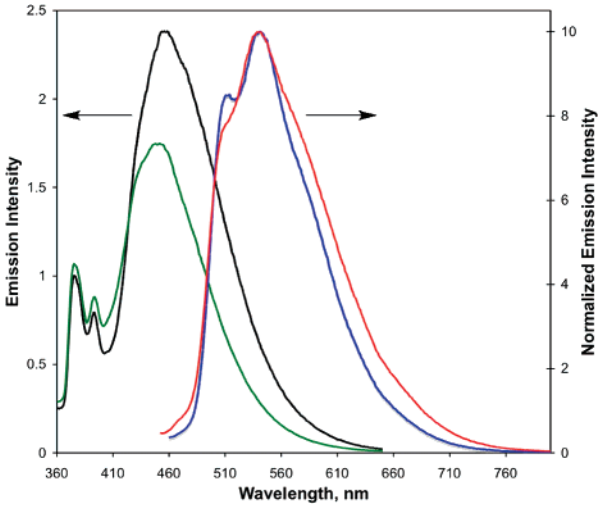

FIGURE 4. The emission spectra of **1** (2×10^{-6} M, $\lambda_{ex} = 390$ nm, blue curve), **2** (2×10^{-6} M, $\lambda_{ex} = 380$ nm, red curve), **6** (1×10^{-5} M, $\lambda_{ex} = 320$ nm, green curve), and **6** + 1 equiv of OH^- (1×10^{-5} M, $\lambda_{ex} = 320$ nm, black) in DMSO solution at 293 K.

ated with the hydrogen bond,[10] the virtually identical features in the emission spectra and related photophysical parameters of **1** and **2** exclude the possibility of the ESIPT process in **1**. However, the emission spectrum of compound **6** in DMSO displays two distinct profiles: one at 378 nm with vibrational structures and small Stokes shift (1163 cm^{-1}) and the other at 454 nm with broad structureless feature and large Stokes shift (5521 cm^{-1}) (see Figure 4). The total emission quantum yield is extremely low in DMSO solution. The different fluorescence excitation spectra monitored at these two wavelengths indicate that the two emission bands do not originate from the same ground-state species. On the other hand, the emission displays a predominant band at 366 nm in nonpolar cyclohexane with a quantum yield of 0.015. Addition of 1 equiv of OH^- to a DMSO solution of **6** resulted in a new absorption band at 404 nm and a bathochromic shift of emission band from 454 to 460 nm with increasing intensity (see Figure 4). Furthermore, the emission band at 378 nm in DMSO completely disappeared and shifted to 512 nm in the presence of 10 equiv of OH^- (see Figure S19). Accordingly, the emission band at 378 nm in DMSO solution is ascribed to the intrinsic fluorescence from **6**, which appears

(10) (a) Scheiner, S. *J. Phys. Chem. A* **2000**, *104*, 5898−5909. (b) Vargas, V. *J. Phys. Chem. A* **2004**, *108*, 281−288. (c) Babara, P. F.; Rentzepis, P. M.; Brus, L. E. *J. Am. Chem. Soc.* **1980**, *102*, 2786−2772.

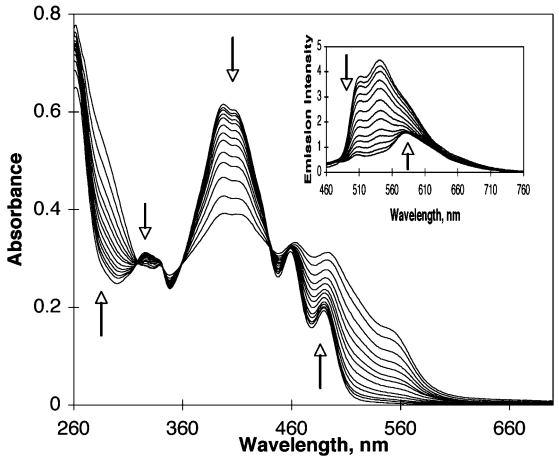

FIGURE 5. Changes of absorption and emission (λ_{ex} = 441 nm) spectra of **1** (1.5×10^{-5} M) on addition of *n*-$Bu_4NH_2PO_4$ ($0-4.2 \times 10^{-3}$ M) in DMSO solution.

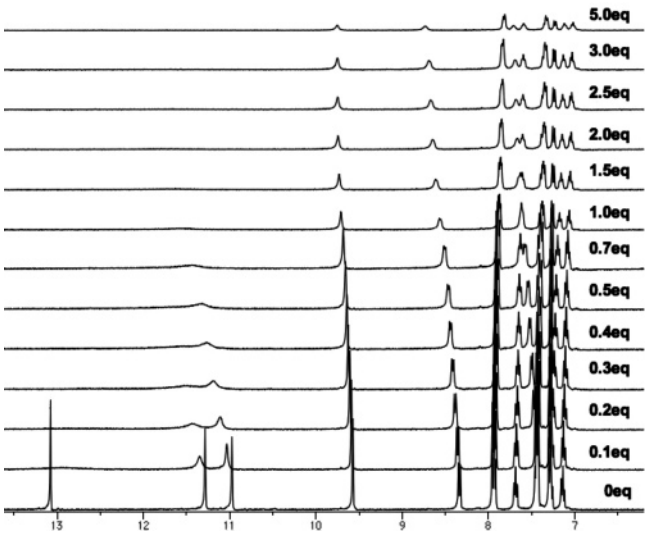

FIGURE 6. Plots of ^{1}H NMR spectra of **1** on addition of *n*-$Bu_4NH_2PO_4$ in DMSO-d_6 solution.

at 366 nm and is the predominant emission in nonpolar cyclohexane solution, while the naphthol proton in compound **6** undergoes partial dissociation in highly polar DMSO solution and the band at 454 nm is assigned to the emission from proton-dissociated **6**.

The tendency of **1** to form aggregated structures in the gas phase has been verified by mass spectrometry (vide supra). The structurally similar **2** also showed effective $\pi-\pi$ stacking in the solid state. However, the concentration-dependent study on the UV−visible absorption spectra of **1** revealed that there is no sign of a newly formed absorption band in the visible region with concentration of compound **1** increasing from 1×10^{-5} to 1×10^{-3} M, which implies that **1** alone apparently is not able to form ground-state aggregate in DMSO solution. The concentration-dependent luminescence experiments with a front-face fluorescence detection mode showed also no difference in emission spectral profiles, which also excludes the possibility of excimer emission at high concentration. The lack of excimer formation is not surprising because of the short excited-state lifetime of probe **1** and, therefore, the rapid excited-state relaxation rate constant over the diffusion rate constant in DMSO

CHART 1

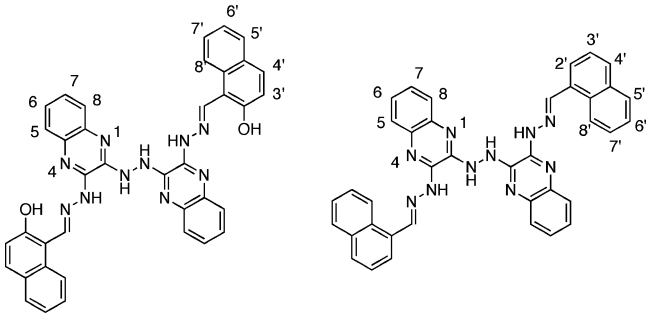

CHART 2

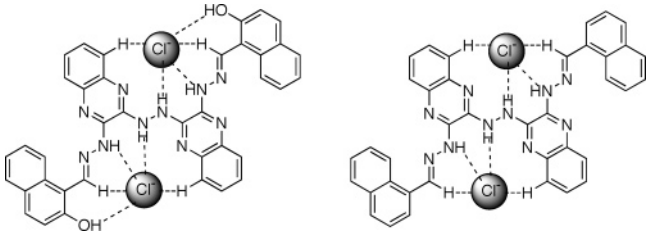

TABLE 3. The Binding Constants, *K* (M^{-2}), Obtained from Fitting of 1:2 Binding Model[a]

probe	anion	log *K*
1	Cl^-	1.8
	OAc^-	7.3
	$H_2PO_4^-$	5.8
2	Cl^-	1.8
	F^-	7.7
	OAc^-	6.6
	$H_2PO_4^-$	5.4

[a] Conditions: probes **1** and **2**, 20 μM in DMSO. Anions were added as tetrabutylammonium salts. The binding constants for Br^-, I^-, HSO_4^-, ClO_4^-, and NO_3^- were not determined due to the very small spectral changes.

solution to prevent the encounter between the excited-state and ground-state molecules.

Anion Sensing Properties. Of the nine anions tested (F^-, Cl^-, Br^-, I^-, OAc^-, $H_2PO_4^-$, HSO_4^-, ClO_4^-, and NO_3^-), only F^-, OAc^-, and $H_2PO_4^-$ generated notable optical spectral changes for **1** and **2**. Moreover, except for the titration with F^- to probe **1**, the patterns of the spectral progressions of **1** or **2** are similar to each other upon the addition of the other two anions. A family of representative absorption and emission spectra of **1** upon the addition of $H_2PO_4^-$ is depicted in Figure 5. The absorption band at 398 nm decreased upon addition of $H_2PO_4^-$, while the band at 490 nm and a shoulder at ~550 nm formed and developed. The color of solution changed from yellow to reddish-brown. The newly appearing bathochromic band on addition of $H_2PO_4^-$ is assigned to a charge transfer from quinoxaline to naphthyl moiety on the basis of semiempirical ZINDO calculation. Concomitant to the absorption spectral changes, the emission band at 542 nm decreased, while a new band at 584 nm developed. The emission color changed from yellowish-green to maroon. As expected from the two potential anion binding pockets within the structures of **1** and **2**, the Job plots revealed a 1:2 binding stoichiometry for both OAc^- and $H_2PO_4^-$ ions. The binding stoichiometry of probe **2** to F^- is also confirmed to be 1:2 by Job plot analysis. The binding constants obtained from a 1:2 model by a spectral fitting procedure using a nonlinear least-square fit algorithm as implemented in the SPECFIT program are collected in Table

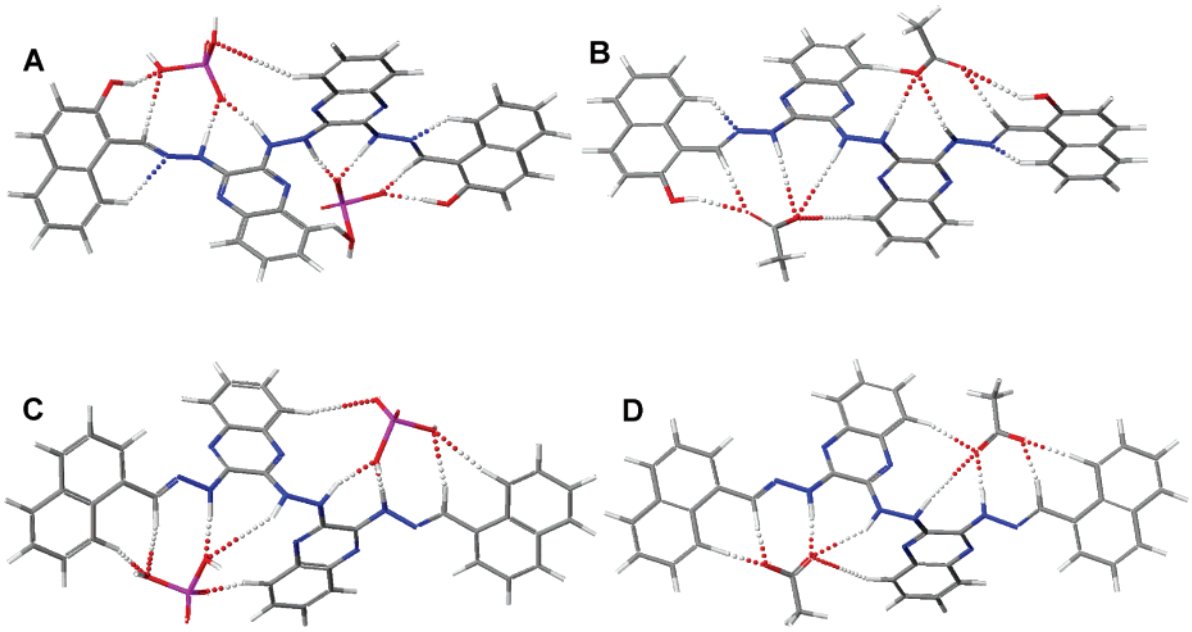

FIGURE 7. Energy-minimized molecular models of **1**•$(H_2PO_4^-)_2$ (A), **1**•$(OAc^-)_2$ (B), **2**•$(H_2PO_4^-)_2$ (C), and **2**•$(OAc^-)_2$ (D).

3.[11] In general, the binding constants of **1** toward anions are slightly higher than the corresponding binding constants of **2**. This may be due to the involvement of hydroxyl groups in the hydrogen bonding, which enables stronger binding affinity toward anions in probe **1** than in probe **2**.

In order to pinpoint the anion receptor sites and fully explore the interaction modes between the anions and probe molecules, we carried out ^{1}H NMR titration experiments in DMSO-d_6 solution. Figure 6 shows the ^{1}H NMR spectra of probe **1** with the addition of $H_2PO_4^-$. As expected from the collective hydrogen bonding interactions, the hydroxyl, hydrazone, hydrazine, and imine protons all underwent noticeable downfield shifts. Moreover, the H_8' protons on naphthyl rings and H_8 protons on quinoxaline also exhibited downfield shift from 8.34 to 8.73 ppm and from 7.29 to 7.81 ppm, respectively, which indicates the formation of C−H····A^- hydrogen bonding interaction (see Chart 1 for the proton number labeling). The rest of the aromatic protons showed upfield shifts owing to the anion-induced through-bond shielding effect.[1b,4e] Similar pattern of proton shifts was also observed with the addition of OAc^- into a DMSO-d_6 solution of probe **1** (see Supporting Information). On the other hand, only the hydroxyl, hydrazone, hydrazine, imine, and quinoxaline H_8 protons displayed downfield shifts with the addition of weakly interacting Cl^- ion (see Supporting Information). Similar anion-induced chemical shifts were also observed in probe **2** with the addition of F^-, OAc^-, $H_2PO_4^-$, and Cl^- (see Supporting Information). The proposed structures of probe−chloride complexes are presented in Chart 2. Given the flexible skeleton of **1** and **2**, it is conceivable that probes **1** and **2** could adopt a conformation to accommodate the strongly interacting anions such as OAc^- or $H_2PO_4^-$ and to compensate the energy required to "twist" the structural framework by forming multiple hydrogen bonds. The energy minimized molecular models of **1**•$(A^-)_2$ and **2**•$(A^-)_2$ derived from semiempirical MOPAC/AM1 method are shown in Figure 7.[12]

The titration profile of probe **1** with F^- is apparently more complicated than others (see Figure 8). Both absorption and emission spectra exhibited two distinct conversion steps. The spectral changes at relatively low concentration of F^- (0−10 equiv) exhibited a series of isosbestic points with new bands formed at 490 and 550 nm. However, a new set of isosbestic points developed with addition of F^- over 10 equiv: the newly developed absorption bands at 490 and 550 nm started to decrease accompanying the growth of a new band at 356 nm. The broad emission band at 596 nm also decreased, and a new band with clear vibrational structure appeared at 512 nm. The sigmoidal binding isotherm in the low fluoride concentration range (below 0.1 mM) suggests that the binding process could be cooperative.[13] Notwithstanding, we realize, in the case where the anion is highly hydrated, the binding isotherm could display sigmoidal curvature.[14] However, we did not observe similar sigmoidal isotherms during the titrations of probes **1** and **2** with all other anions under the same experimental conditions. Moreover, the sigmoidal isotherms were still observed in the control experiments conducted either with vigorously predried anion samples in anhydrous DMSO solution under anaerobic condition or in 1% H_2O/DMSO solution. In addition, unlike other probe−anion interactions showing 1:2 stoichiometry, the Job plot of probe **1** and fluoride gave a 1:1 interacting stoichiometry.

Attempts to monitor the solution equilibrium process by ^{1}H NMR titration yielded little information about the possible structure of the new species formed in solution. The high probe concentration (2−10 mM) employed in the ^{1}H NMR experiments resulted in very complicated and broad spectral patterns

(11) (a) *SPECFIT*, version 3.0; Spectra Software Associates: Claix, France, 2005. (b) Gampp, H.; Maeder, M.; Meyer, C. J.; Zuberbühler, A. D. *Talanta* **1985**, *32*, 95−101. (c) Gampp, H.; Maeder, M.; Meyer, C. J.; Zuberbühler, A. D. *Talanta* **1986**, *33*, 943−951.

(12) *CAChe 5.0* for Windows; Fujitsu Ltd., 2001.

(13) Connors, K. A. *Binding Constants*; John Wiley and Sons: New York, 1987.

(14) The commercially sold tetrabutylammonium fluoride from the Acros company contains three cocrystallized water.

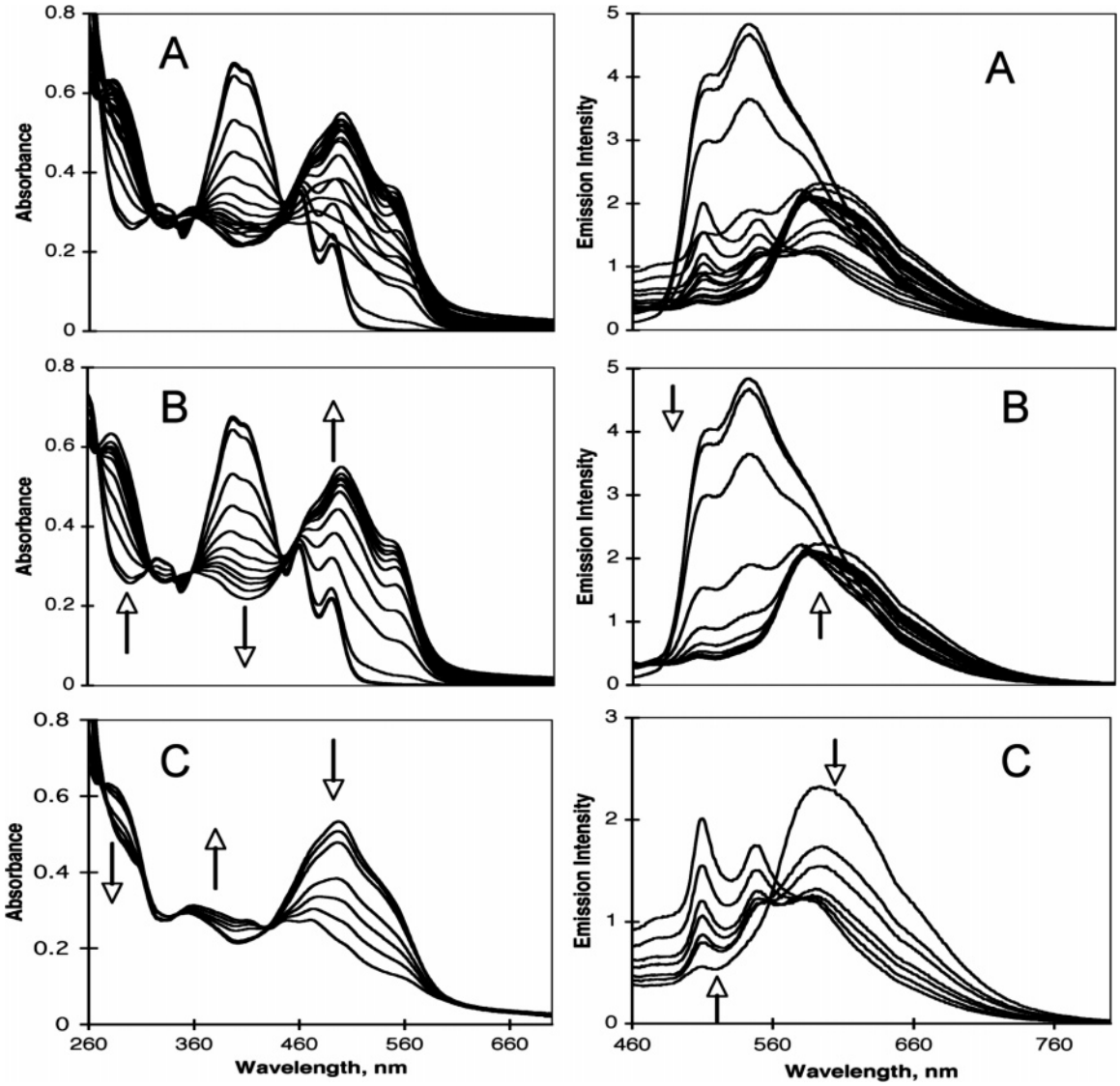

FIGURE 8. Absorption (left) and emission (right) spectra of **1** (1.5×10^{-5} M) on addition of *n*-Bu_4NF in DMSO solution: (A) $[F^-] = 0-4.4 \times 10^{-3}$ M; (B) $[F^-] = 0-1.0 \times 10^{-4}$ M; (C) $[F^-] = 3.8 \times 10^{-4}-4.4 \times 10^{-3}$ M; $\lambda_{ex} = 441$ nm.

on addition of F^- ion, which indicated that highly aggregated species appeared in solution in the presence of F^-. Subsequently, compound **3** was titrated with F^- to serve as a model for probe **1**. Figure 9 shows the ^1H NMR titration of a DMSO-d_6 solution of compound **3** with F^-. In contrast to the appearance of possible aggregated species from probe **1** in the presence of F^-, addition of F^- into a DMSO solution of **3** showed no sign of aggregation judged from the sharp proton peaks. This observation implies that the less π-extended structure of **3** is not prone to form noticeable intermolecular $\pi-\pi$ interaction when compared to probe **1**. The hydroxyl and hydrazone proton signals became broad, and the imine proton signal moved to downfield position with concomitant upfield shifts of all other aromatic proton signals upon the addition of F^- up to 2 equiv, a typical phenomenon for hydrogen bonding interaction with incoming F^-. The imine proton peak started to move to upfield position with addition of F^- over 2 equiv. This observation is consistent with a neat deprotonation process of the most acidic hydroxyl O−H to form the HF_2^- anion.[7] The overall process can be expressed in Scheme 2.

Previously, Yoon and co-workers reported an elegantly designed chemosensor comprising dipyridyl amine functionalized naphthalene bisimide, which is capable of selectively sensing pyrophosphate by formation of a [2 + 2] type complex and generates naphthalene bisimide based excimer emission.[15] Several similar [2 + 2] type supramolecular complexes have also been reported for recognition of either metal cations or fullerene under certain experimental conditions with judiciously designed sensing molecules. For examples, a fluorescence turn-on coumarin azacrown-based chemosensor designed by Chen and Huang showed an exclusive selectivity to Pb^{2+} ion by formation of a [2 + 2] complex through a crown−ketoester cooperative chelation effect to Pb^{2+} ion.[3m] Licchelli and co-workers reported a simple bis-15-crown naphthalenediimide to selectively bind Ba^{2+} ion to form a [2 + 2] sandwich-like complex with enhanced excimer emission.[16] A recent report by Martín and co-workers described a tetrathiafulvalene derivative

(15) Lee, H. N.; Xu, Z.; Kim, S. K.; Swamy, K. M. K.; Kim, Y.; Kim, S.-J.; Yoon, J. *J. Am. Chem. Soc.* **2007**, *129*, 3828−3829.

(16) Licchelli, M.; Biroli, A. O.; Poggi, A. *Org. Lett.* **2006**, *8*, 915−918.

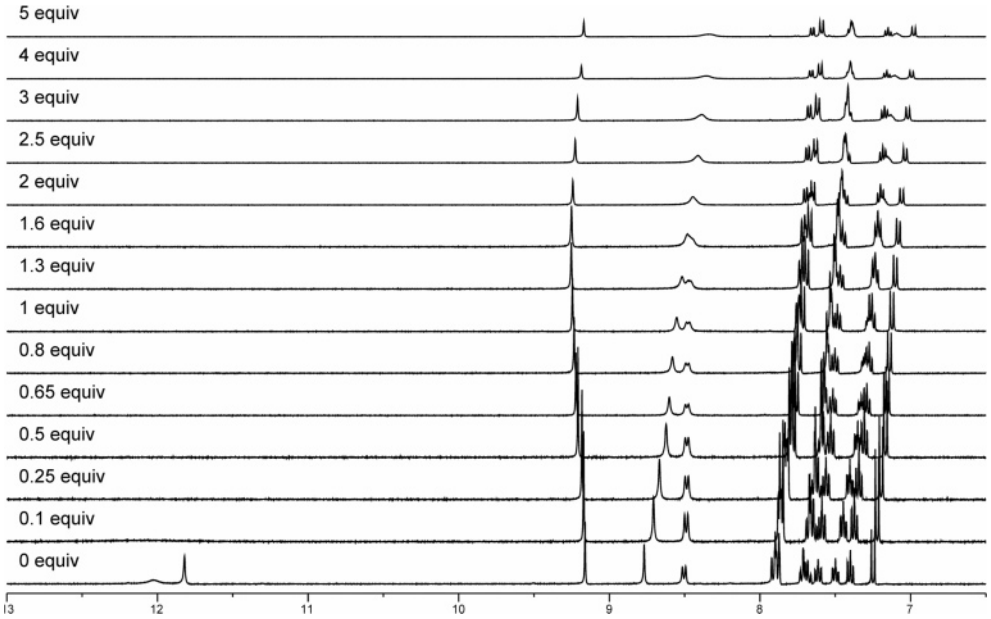

FIGURE 9. Plots of ^{1}H NMR spectra of compound **3** on addition of F^- in DMSO-d_6.

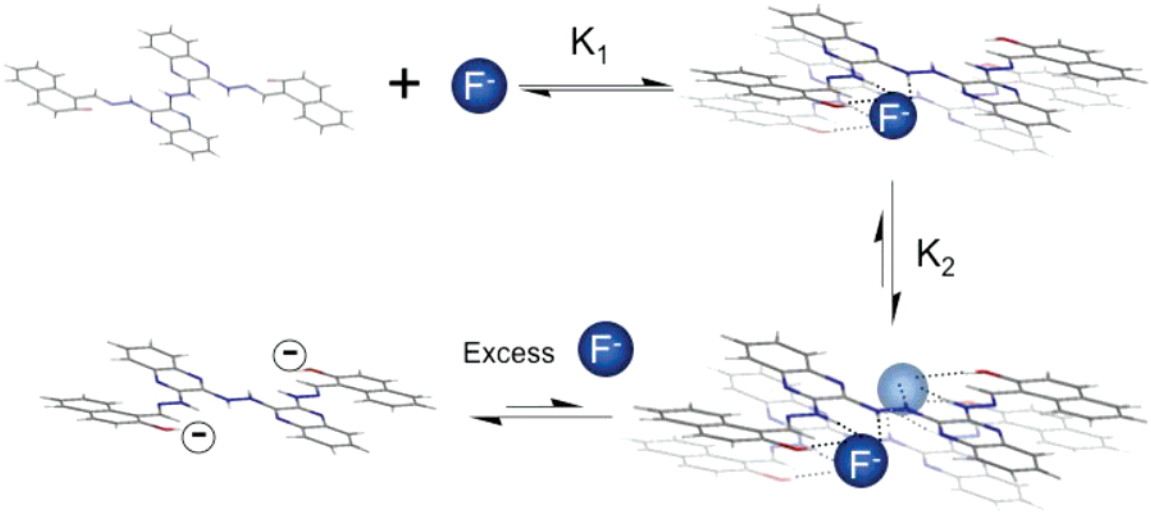

FIGURE 10. The formation mechanism of proposed [2 + 2] supramolecular complex and the excess fluoride-induced deprotonation. The [2 + 1] complex would immediately convert to the [2 + 2] complex and not be able to accumulate in solution. See text for more details.

SCHEME 2

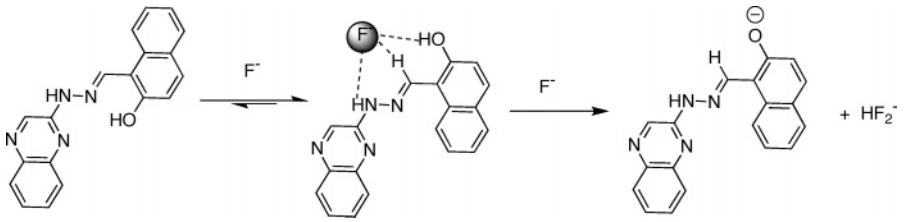

to be an effective receptor for fullerene. They have found that the binding stoichiometry can be varied under solvent control. In a $CHCl_3/CS_2$ mixture, the reported tetrathiafulvalene derivative receptor binds fullerene in a [2 + 2] fashion and shows positive homotropic cooperativity.[3a]

To account for the absorption and emission spectral changes of probe **1** on addition of F^-, we tentatively propose the formation of a [2 + 2] fluoride-induced associated dimer complex via a combination of multiple hydrazine/hydrazone/imine/hydroxyl anion hydrogen bonding and $\pi-\pi$ stacking interactions between probe **1** and F^-. The formation of the [2 + 2] complex is confirmed by ESI mass spectrometry (vide infra). Figure 10 illustrates the possible formation mechanism of the proposed fluoride-induced [2 + 2] supramolecular complex. In the present case, the association of a first F^- anion to form a dimeric aggregate allows for the association of a second F^- anion with the preorganized hydrogen bonding pocket and is expected to exert a cooperative effect. The emission decay

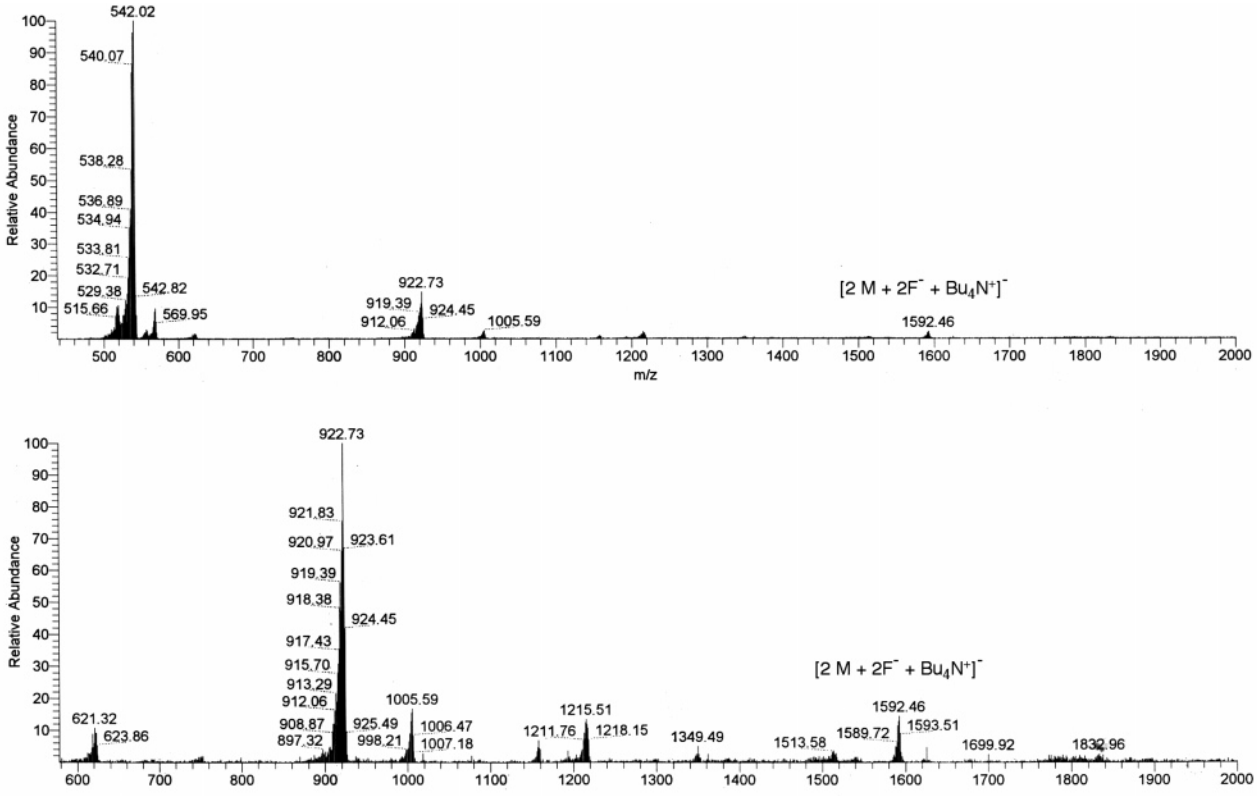

FIGURE 11. Negative mode ESI mass spectrum of probe **1** on addition of 0.5 equiv of F^- showing the formation of the [2 + 2] supramolecular complex with a molecular peak at $m/z = 1592.46$.

profile at the newly developed band at 600 nm on addition of 1 equiv of F^- required a biexponential fitting with excited-state lifetimes of 2.8 and 0.13 ns. The shorter-lived component is apparently from the free probe **1**, and the longer-lived component is attributed to the probe **1**−fluoride associated complex.[15,17] The lack of a negative pre-exponential coefficient in the time-resolved decay profile of the longer-lived component suggests that the emission originates from the direct photoexcitation of a ground-state-associated dimer instead of from a species generated in the excited state.[18]

The appearance of an emission at shorter wavelength with a single-exponential decay of excited-state lifetime of 160 ps is monitored at 500 nm in the presence of 300 equiv of F^-. Addition of 100 equiv of *n*-Bu_4OH into a DMSO solution of probe **1** resulted in a similar emission spectrum with an excited-state lifetime of 190 ps when monitored at 500 nm (see Figure S20 for the changes of emission spectra of probe **1** on addition of *n*-Bu_4OH in DMSO solution). Thus, the short wavelength emission band that appeared after addition of excess fluoride is considered to be the consequence of deprotonation of naphthalenol moieties that generate the electrostatic repulsion between negative charged **1** and subsequently disassemble the associated dimer complex. Finally, the molecular peak with $m/z = 1592.46$ corresponding to the formula of the [2 + 2] supramolecular dimer $[2M + 2F^- + Bu_4N^+]^-$ (calcd $m/z = 1592.76$) was observed from negative mode ESI mass spectrometry with the addition of 0.5 equiv of F^- into a DMSO solution of probe **1** (see Figure 11). However, only deprotonated **1** was observed from the ESI mass spectra upon addition of F^- over 0.5 equiv into a DMSO solution of probe **1**. This result is not totally unexpected considering the strong basicity of F^- in the gas phase, which strongly facilitates the deprotonation process.

The proof of formation of a fluoride-induced supramolecular complex in solution is further supported by pulsed-field gradient (PFG) NMR spectroscopy, a diffusion NMR technique. PFG NMR has been particularly useful for the determination of a supramolecular system in solution.[19] PFG NMR is capable of identifying the size and possible shape of different supramolecular systems on the basis of measured diffusion coefficients.[20] Figure 12 demonstrates the results obtained from PFG NMR measurements. The diffusion coefficient of solution species after addition of 0.5 equiv of fluoride becomes 1.43×10^{-10} m^2/s, which is smaller than the diffusion coefficient (1.81×10^{-10} m^2/s) of free probe **1**. This result clearly demonstrates that a larger sized aggregated species appears after addition of fluoride.

The diffusion coefficient can be related to the particle size using the Stokes−Einstein equation, $D = k_BT/6\pi\eta r$, to determine

(17) (a) Shazmann, B.; Alhashimy, N.; Diamond, D. *J. Am. Chem. Soc.* **2006**, *128*, 8607−8614. (b) Kim, S. K.; Bok, J. H.; Bartsch, R. A.; Lee, J. Y.; Kim, J. S. *Org. Lett.* **2005**, *7*, 4839−4842. (c) Lee, S. H.; Kim, S. H.; Kim, S. K.; Jung, J. H.; Kim, J. S. *J. Org. Chem.* **2005**, *70*, 9288−9295. (d) Kim, S. K.; Lee, S. H.; Lee, J. Y.; Lee, J. T.; Bartsch, R. A.; Kim, J. S. *J. Am. Chem. Soc.* **2004**, *126*, 16499−16506. (e) Nishizawa, S.; Kato, Y.; Teramae, N. *J. Am. Chem. Soc.* **1999**, *121*, 9463−9464.

(18) Winnik, F. M. *Chem. Rev.* **1993**, *93*, 587−614.

(19) (a) Pregosin, P. S.; Kumar, P. G.; Fernández, I. *Chem. Rev.* **2005**, *105*, 2977−2998 and references cited therein. (b) Cohen, Y.; Avram, L.; Frish, L. *Angew. Chem., Int. Ed.* **2005**, *44*, 520−554 and references cited therein.

(20) (a) Allouche, L.; Marquis, A.; Lehn, J.-M. *Chem.—Eur. J.* **2006**, *12*, 7520−7525. (b) Otto, W. H.; Keefe, M. H.; Splan, K. E.; Hupp, J. T.; Larive, C. K. *Inorg. Chem.* **2002**, *41*, 6172−6174. (c) Beves, J. E.; Constable, E. C.; Housecroft, C. E.; Neuburger, M.; Schaffner, S.; Shardlow, E. J. *Dalton Trans.* **2007**, 1593−1602. (d) Evan-Salem, T.; Frish, L.; van Leeuwen, F. W. B.; Reinhoudt, D. N.; Verboom, W.; Kaucher, M. S.; Davis, J. T.; Cohen, Y. *Chem.—Eur. J.* **2007**, *13*, 1969−1977.

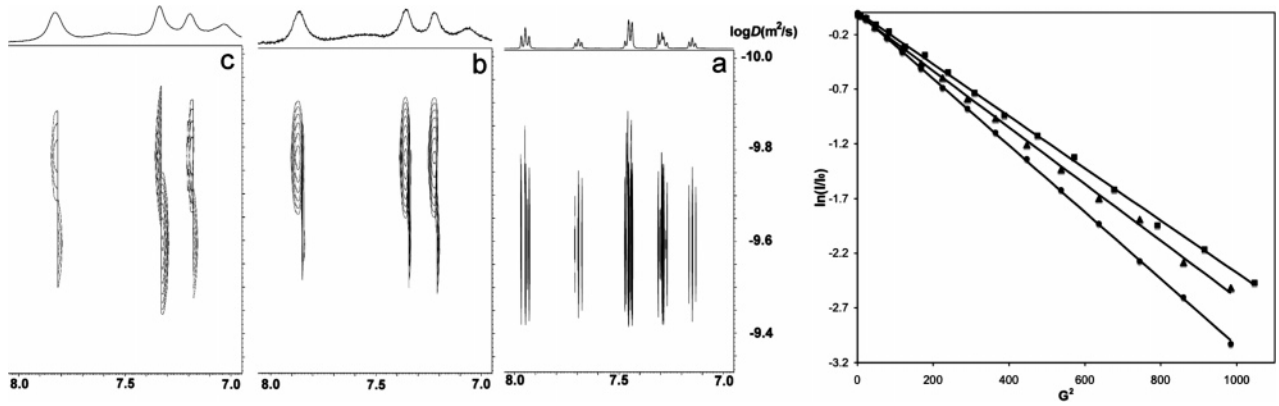

FIGURE 12. Left: ^{1}H DOSY spectra of probe **1** (a), probe **1** + 0.5 equiv of F^- (b), and probe **1** + excess F^- (c). Right: plots of intensity decay with gradient strength (bottom) for probe **1** (sphere), probe **1** + 0.5 equiv of F^- (square), and probe **1** + excess F^- (triangle).

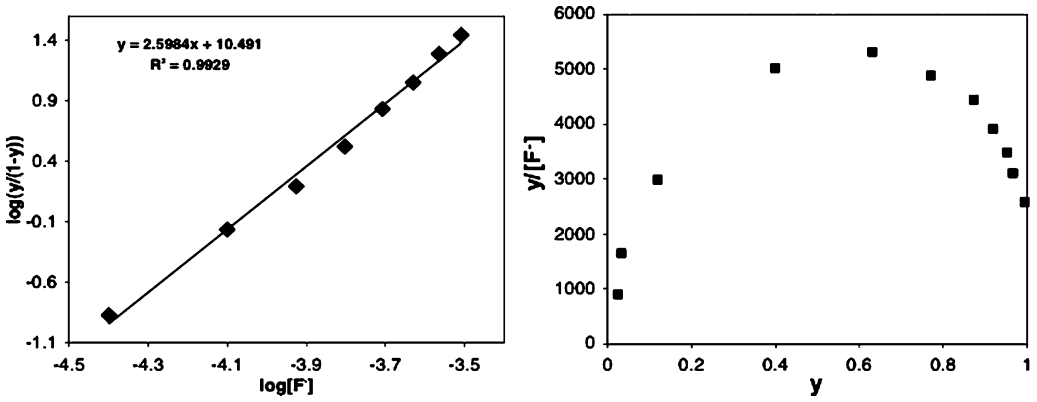

FIGURE 13. Hill plot (left) and Scatchard plot (right) for the binding of F^- to probe **1** based on the UV−vis spectral changes in the low fluoride concentration range.

the hydrodynamic radius where T is absolute temperature, k_B is Boltzmann's constant, r is the hydrodynamic radius, and η is the solvent viscosity.[21] The calculated hydrodynamic radii for probe **1** and the fluoride-induced complex are 11.0 and 13.9 Å, respectively, which are larger than the molecular radii of probe **1** (5.7 Å) and the proposed fluoride-induced dimer (6.5 Å) obtained from molecular modeling. It should be noted here that the Stokes−Einstein equation is derived for a spherical particle. For a non-spherical particle, the frictional coefficient is larger than $6\pi\eta r$ and the calculated hydrodynamic radius is expected to be larger than the molecular radius.[21] Notwithstanding, the formation of higher order aggregates in solution cannot be completely ruled out, especially at higher probe concentration carried out in the ^{1}H NMR experiments. On the basis of the observation of the peak assignable to the dimeric structure from ESI mass spectrometry that was also performed under dilute conditions, the simplest dimeric structure would be most likely formed under our dilute experimental conditions with the concentration of probe molecule around 1.5×10^{-5} M for absorption and fluorescence titrations and fits our results satisfactorily. Interestingly, addition of excess fluoride results in an intermediate diffusion coefficient (1.59×10^{-10} m^2/s) between free probe **1** and species formed with addition of 0.5 equiv of fluoride, which suggests that the smaller deprotonated species (compared to the larger supramolecular aggregate) appears in solution at high fluoride concentration and results in a larger diffusion coefficient than the condition where the supramolecular aggregate is a dominant species.

Subsequently, the cooperative anion binding was analyzed with the Hill equation: $\log[y/(1-y)] = n\log[\text{anion}] + \log K$, where y is the fractional occupancy of the host, n is the Hill coefficient, and K is the apparent binding constant.[13] The Hill coefficient is best thought of as an interaction coefficient reflecting the extent of cooperativity with a maximum value equal to the number of binding sites.[3a,13] The Hill plot for the binding of F^- to **1** based on the UV−visible spectral changes at low fluoride concentration range is shown in Figure 13. The high Hill coefficient ($n = 2.6$) of probe **1** for fluoride indicates that more than two active sites participate in the binding process and, thus, strongly suggest the formation of an anion-induced supramolecular dimer, which provides four potential binding sites available for incoming fluoride, as illustrated in Figure 10.

Scatchard plot was further employed to characterize the binding (see also Figure 13). The Hill coefficient is correlated with the maximum value (y_{max}) in the Scatchard plot with $n = 1/(1 - y_{max})$.[4i,13] The positive and negative cooperativities are characterized by the upward and downward curvatures, respectively, in the Scatchard plots.[3a,13] As expected, the y_{max} value shows a maximum at 0.63 with upward curvature shape which together with the large Hill coefficient is in agreement with a positive cooperative binding event. The binding of the first fluoride to form a preorganized supramolecular structure greatly facilitates the inclusion of second fluoride via a cooperative

(21) Cussler, E. L. *Diffusion: Mass Transfer in Fluid Systems*; Cambridge University Press: Cambridge, 1984.

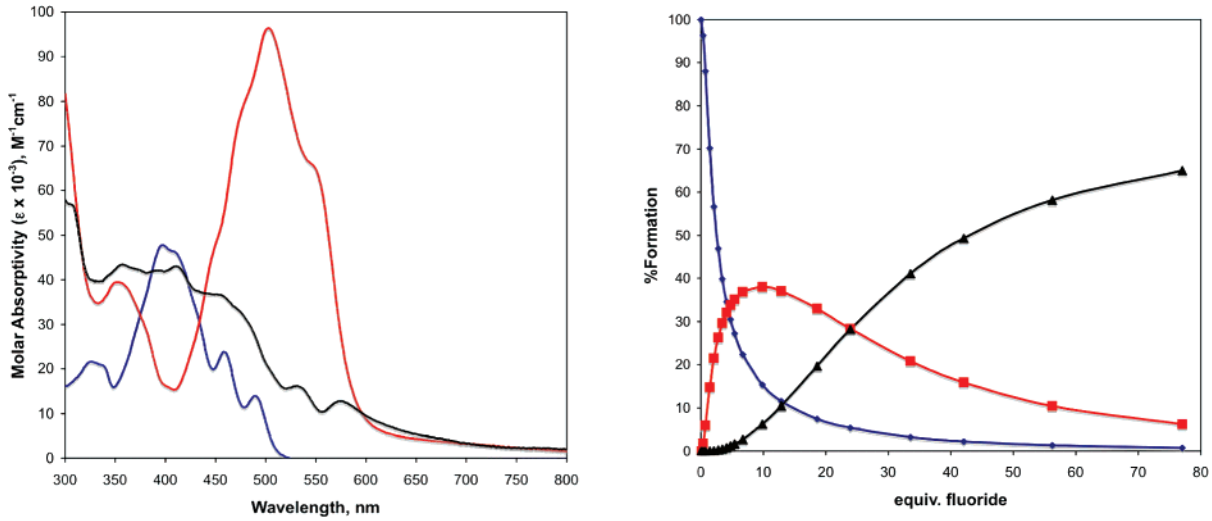

FIGURE 14. The absorption spectra (left) and % formation versus equiv of F^- addition (right) for probe **1** (blue curve), [2 + 2] complex (red curve), and deprotonated probe **1** [**1** − H]$^-$ (black line).

process. The concentration distributions and deconvoluted spectra, as illustrated in Figure 14, of the three color species involved (free probe **1**, fluoride-induced dimeric probe **1**, and deprotonated probe **1**) can be obtained by spectral deconvolution over the entire wavelength range using a nonlinear least-square fit algorithm, as implemented in the SPECFIT software package.[11] The overall binding constants (log K_1K_2) for F^- and the final deprotonation step (log K_3) were also extracted from the same spectral deconvolution process to give log $K_1K_2 = 12.7$ M^{-3} and log $K_3 = 5.6$ M. The failure to obtain a reasonable fitting for individual K_1 and K_2 implies a strongly cooperative behavior with $K_2 >> K_1$ and further indicates that the concentration of the 2:1 intermediate is not able to accumulate in solution before further rapid formation of the final [2 + 2] complex.[3b]

Conclusion

In summary, we have demonstrated that probes **1** and **2** represent a new type of colorimetric and fluorescence probes for detecting inorganic anions such as F^-, OAc^-, and $H_2PO_4^-$ ions. In particular, probe **1** exhibits positive homotropic cooperativity with high sensitivity and selectivity to fluoride under visible light excitation and represents a rare example in the literature for the anion sensing system with such a unique anion−probe interacting mechanism. The simple and high yield synthesis of probes of this kind and their facile modification of the structural framework of **1** and **2** can thus principally produce libraries for potentially different receptors and promise a new design direction for effective optical anion sensing systems in the future.

Experimental Section

Materials and General Procedures. 2,3-Dichloroquinoxaline was synthesized according to a published method.[22] All other chemical reagents were commercially available and were used without further purification unless otherwise noted. NMR spectra were recorded on either a Bruker AMX400 (400.168 MHz for ^{1}H NMR and 100.622 MHz for ^{13}C NMR) or a Bruker AV400 (400.168 MHz for ^{1}H NMR and 100.622 MHz for ^{13}C NMR). ^{1}H and ^{13}C NMR chemical shifts are reported in parts per million downfield from tetramethylsilane (TMS, δ scale) with the solvent resonances as internal standards. Absorption spectra were obtained using a Perkin-Elmer Lambda 900 UV−visible−NIR spectrophotometer. Emission spectra were recorded in an air-equilibrated DMSO solution at 298 K with a Fluorolog III photoluminescence spectrometer. Luminescence quantum yields were calculated relative to 9,10-diphenylanthracene in cyclohexane solution ($\Phi_{em} = 0.9$). Corrected emission spectra were used for the quantum yield measurements. Luminescence quantum yields were taken as the average of three separate determinations and were reproducible to within 10%.

Semiempirical MOPAC calculations were performed to obtain the energy-minimized probe−anion structures with the PM3 parameter set implemented in the program package Quantum CAChe. Semiempirical ZINDO calculations were performed to estimate the electron density distribution of the HOMO and LUMO orbitals. The structure was first optimized by semiempirical AM1 calculations. Subsequently, the difference between electron affinity and ionization potential was calculated employing ZINDO using the program package Quantum CAChe.

Fluorescence lifetimes were measured on an Edinburgh Instruments Mini-τ single-photon-counting lifetime spectrometer. The samples were excited at 370 nm from a diode laser with a 80 ps pulse width. Nonlinear least-squares fittings of the decay curves were performed with the Levenburg−Marquardt algorithm and implemented by the Edinburgh Instruments T900 software.

Alternately, luminescence lifetimes were determined on an Edinburgh FL920 time-correlated pulsed single-photon-counting instrument. Samples were excited at 337 nm from a nitrogen-pulsed flashlamp with 1 ns fwhm pulse duration transmitted through a Czerny−Turner design monochromator. Emission was detected at 90° via a second Czerny−Turner design monochromator onto a thermoelectrically cooled red-sensitive photomultiplier tube. The resulting photon counts were stored on a microprocessor-based multichannel analyzer. The instrument response function was profiled using a scatter solution and subsequently deconvoluted from the emission data to yield an undisturbed decay. Nonlinear least-squares fittings of the decay curves were performed with the Levenburg−Marquardt algorithm and implemented by the Edinburgh Instruments F900 software.

Single crystal of **2** or **4** were mounted on a glass fiber using oil. All measurements were made on a Bruker X8 Apex CCD area detector equipped with graphite-monochromated Mo Kα radiation.

(22) (a) Okafor, C. O. *J. Heterocycl. Chem.* **1980**, *17*, 149−153. (b) Okafor, C. O. *J. Heterocycl. Chem.* **1979**, *16*, 1025−1027.

The structures were solved by direct methods[23] and refined by a full-matrix least-squares technique based on F^2 using the SHELXL97 program.[23b] The non-hydrogen atoms were refined anisotropically. Hydrogen atoms were included in idealized positions but not refined. All calculations were performed using the Bruker SHELX-TL crystallographic software package.[24]

Absorption and fluorescence anion titrations were performed using a 2.5 mL chemosensor solution in DMSO titrated with a sample of the anions prepared with the same chemosensor solution. Absorption and emission spectra were recorded following each addition of anion. The apparent association constants, *K*, and Hill coefficients, *n*, were determined by Hill eq 1:

$$\log(y/(1-y)) = n\log[\text{anion}] + \log K \quad (1)$$

where $y = A/(A_{max} - A_0)$, A is the absorbance at 560 nm at any given fluoride concentration, A_0 is the absorbance at 560 nm in the absence of fluoride, and A_{max} is the maxima absorbance at 560 nm in the presence of fluoride in solution.[3m,13]

The association constants, *K*, listed in Table 3 were determined from a 1:2 stoichiometry (probe to anion) by fitting the whole series of spectra at 1 nm intervals using the software SPECFIT 3.0 from Spectrum Software Associates, which employs a global system with expanded factor analysis and Marquardt least-squares minimization to obtain globally optimized parameters.[11] ^{1}H NMR titration experiments were carried out in DMSO-d_6 solution at 1−5 mM concentration of the probe molecules.

^{1}H NMR diffusion experiments were performed by using a Bruker DRX 500 MHz spectrometer equipped with a gradient system capable of producing magnetic-field pulse gradients in the *z*-direction of about 52 Gcm^{-1}. Diffusion measurements were performed by using a stimulated echo sequence (STE). All ^{1}H FIDs were acquired at 298 K. Experiments were carried out with a relaxation delay of 2 s, a diffusion delay (Δ) of 50 ms, and a gradient pulse duration (δ) of 7 ms. Gradient amplitudes were varied from 0.66 to 32.4 Gcm^{-1}. Individual FIDs were processed using Bruker TOPSPIN 2.0 software.

Synthesis. Compound 4. A mixture of 2,3-dichloroquinoxaline (10 g, 0.05 mol) and hydrazine hydrate (50 mL) was placed in a reaction flask. The solution was refluxed for 5 days. The yellow precipitate was collected by filtration and washed with methanol and recrystallized from DMF to give a yellow powder of **4** (7.8 g, 90%): ^{1}H NMR (400 MHz, DMSO-d_6) δ 10.8 (2 H, s), 8.92 (2 H, s), 7.27 (2 H, d, J = 7.6 Hz), 7.21 (2 H, d, J = 7.7 Hz), 7.05 (2 H, d, J = 7.5 Hz), 6.97 (2 H, d, J = 7.6 Hz), 4.54 (4 H, s); ^{13}C NMR (100 MHz, DMSO-d_6) δ 150.6, 137.9, 134.0, 129.3, 124.9, 123.7, 122.2, 114.2; HREIMS *m*/*z* 348.1566 (calcd *m*/*z* 348.1559 for M$^+$); Anal. Calcd for $C_{16}H_{16}N_{10}$: C, 55.16; H, 4.63; N, 40.21. Found: C, 54.93; H, 4.72; N, 40.36.

Compound **5** was prepared in a similar manner to compound **4** by refluxing 2-chloroquinoxaline in hydrazine hydrate for 5 days. Recrystallization from CH_3OH afforded a yellow powder of **5** in 82% yield: ^{1}H NMR (400 MHz, DMSO-d_6) δ 8.68 (1 H, s), 8.36 (1 H, s), 7.77 (1 H, d, J = 8.0 Hz), 7.76−7.54 (2 H, m), 7.35−7.30 (1 H, m), 4.44 (2 H, s); ^{13}C NMR (100 MHz, DMSO-d_6) δ 153.9, 141.5, 138.3, 136.6, 129.6, 128.4, 125.4, 123.4; HREIMS *m*/*z* 160.0749 (calcd *m*/*z* 160.0749 for M$^+$). Anal. Calcd for $C_8H_8N_4$: C, 59.99; H, 5.03; N, 34.98. Found: C, 59.89; H, 5.21; N, 35.15.

(23) Sheldrick, G. M. *SHELXS97, Program for Crystal Structure Solution*; University of Göttingen: Göttingen, Germany, 1997. (b) Sheldrick, G. M. *SHELXL97, Program for Crystal Structure Solution*; University of Göttingen: Göttingen, Germany, 1997.

(24) *Shelxtl for WindowsNT: Crystal Structure Analysis Package*; Bruker: Madison, WI, 1997.

Compound 1. A mixture of **4** (1.0 g, 2.87 mmol) and 2-hydroxy-1-naphthaldehyde (0.98 g, 5.74 mmol) was placed in a reaction flask containing 100 mL of methanol. The solution was then refluxed for 48 h. The resulting orange precipitate was collected by filtration and washed with methanol and recrystallized from DMF/ether to give orange powder of **1** (1.7 g, 90%): ^{1}H NMR (400 MHz, DMSO-d_6) δ 13.1 (2 H, s) 11.3 (2 H, s), 11.0 (2 H, s), 9.57 (2 H, s), 8.34 (2 H, d, J = 8.6 Hz), 7.93 (4 H, m), 7.69 (2 H, t, J = 7.4 Hz), 7.43 (6 H, m), 7.29 (4 H, m), 7.13 (2 H, t, J = 7.3 Hz); ^{13}C NMR (100 MHz, DMSO-d_6) δ 157.5, 144.5, 144.1, 137.2, 132.8, 132.0, 131.4, 129.2, 128.9, 127.7, 127.6, 125.7, 125.1, 123.4, 122.3, 120.5, 118.9, 114.1, 108.8; HRFABMS *m*/*z* 657.2477 (calcd *m*/*z* 657.2475 for M + H$^+$). Anal. Calcd for $C_{38}H_{28}N_{10}\cdot 3H_2O$: C, 67.24; H, 5.05; N, 20.64. Found: C, 67.03; H, 4.67; N, 20.40.

Compound 2. A mixture of **4** (1.0 g, 2.87 mmol) and 1-naphthaldehyde (0.90 g, 5.74 mmol) was placed in a reaction flask containing 100 mL of methanol. The solution was then refluxed for 48 h. Subsequently, the red precipitate was collected by filtration and washed with methanol and recrystallized from DMF/ether to give a red powder of **2** (1.7 g, 95%): ^{1}H NMR (400 MHz, DMSO-d_6) δ 11.2 (2 H, s), 11.1, (2 H, s), 9.42 (2 H, s), 8.92 (2 H, d, J = 8.5 Hz), 8.12 (2 H, d, J = 6.1 Hz), 8.04 (4 H, d, J = 8.1 Hz), 7.75 (2 H, t, J = 7.5 Hz), 7.66 (4 H, m), 7.50 (2 H, d, J = 7.8 Hz), 7.45 (2 H, d, J = 7.8 Hz), 7.24 (2 H, t, J = 7.3 Hz), 7.12 (2 H, t, J = 7.5 Hz); ^{13}C NMR (100 MHz, DMSO-d_6) δ 145.05, 145.02, 137.3, 133.5, 133.0, 130.2, 130.0, 129.9, 129.1, 128.7, 127.1, 126.5, 126.1, 125.7, 125.6, 124.9, 124.0, 122.1, 114.0; HRFABMS *m*/*z* 625.2585 (calcd *m*/*z* 625.2577 for M + H$^+$). Anal. Calcd for $C_{38}H_{28}N_{10}\cdot 2.5H_2O$: C, 68.15; H, 4.97; N, 20.91. Found: C, 68.08; H, 4.69; N, 20.95.

Compound 3. A mixture of **5** (1.0 g, 6.24 mmol) and 1-naphthaldehyde (1.1 g, 6.39 mmol) was placed in a reaction flask containing 100 mL of methanol. The solution was then refluxed for 48 h. Subsequently, the red precipitate was collected by filtration and washed with methanol and recrystallized from DMF/ether to give a yellow powder of **3** (1.7 g, 88%): ^{1}H NMR (400 MHz, DMSO-d_6) δ 11.9 (2 H, br s), 9.17, (1 H, s), 8.76 (1 H, s), 8.49 (1 H, d, J = 6.8 Hz), 7.89−7.86 (3 H, m), 7.70−7.67 (2 H, m), 7.61 (1 H, t, J = 6.3 Hz), 7.48 (1 H, br s), 7.39 (1 H, t, J = 6.1 Hz), 7.24 (1 H, d, J = 7.0 Hz); ^{13}C NMR (100 MHz, DMSO-d_6) δ 156.9, 149.0, 142.1, 141.1, 137.8, 136.8, 131.8, 131.2, 130.4, 128.8, 128.7, 128.0, 127.6, 126.4, 125.2, 123.4, 124.8, 118.6, 109.8; HREIMS *m*/*z* 314.1161 (calcd *m*/*z* 314.1168 for M$^+$). Anal. Calcd for $C_{19}H_{14}N_4O$: C, 72.60; H, 4.49; N, 17.82. Found: C, 72.61; H, 4.40; N, 17.85.

Compound 6. To 100 mL of methanol were added 1-naphthaldehyde (100 mg, 0.58 mmol) and hydrazine hydrate (0.2 mL), and the mixture was refluxed under nitrogen for 6 h. The volatile was removed under reduced pressure, and the residue was washed with hexane to afford a yellow powder of **6** (82 mg, 76%): ^{1}H NMR (400 MHz, DMSO-d_6) δ 12.7 (1 H, br s), 8.86, (1 H, s), 8.08 (1 H, d, J = 6.8 Hz), 7.81 (1 H, d, J = 6.3 Hz), 7.73 (1 H, d, J = 7.1 Hz), 7.50 (1 H, t, J = 6.2 Hz), 7.33 (1 H, t, J = 6.1 Hz), 7.11 (1 H, d, J = 7.1 Hz), 6.98 (2 H, s); ^{13}C NMR (100 MHz, DMSO-d_6) δ 156.1, 139.8, 130.8, 129.7, 128.7, 127.7, 126.9, 123.0, 120.4, 118.6, 109.6; HREIMS *m*/*z* 187.0874 (calcd *m*/*z* 187.0871 for M + H$^+$). Anal. Calcd for $C_{11}H_{10}N_2O$: C, 70.95; H, 5.44; N, 15.04. Found: C, 70.58; H, 5.38; N, 15.09.

Acknowledgment. We thank the National Science Council in Taiwan (Grants 94-2113-M-001-014 and 95-2113-M-001-033-MY2) and Academia Sinica for support of this research.

Supporting Information Available: X-ray crystallographic details of **2** and **4** in cif format, ^{1}H and ^{13}C NMR spectra of all new compounds, and additional anion titration spectra. This material is available free of charge via the Internet at http://pubs.acs.org.

JO7019916